Unveiling Extensive Clouds of Dark Gas in the Solar Neighborhood

Isabelle A. Grenier,[1]* Jean-Marc Casandjian,[1,2] Régis Terrier[3]

From the comparison of interstellar gas tracers in the solar neighborhood (HI and CO lines from the atomic and molecular gas, dust thermal emission, and γ rays from cosmic-ray interactions with gas), we unveil vast clouds of cold dust and dark gas, invisible in HI and CO but detected in γ rays. They surround all the nearby CO clouds and bridge the dense cores to broader atomic clouds, thus providing a key link in the evolution of interstellar clouds. The relation between the masses in the molecular, dark, and atomic phases in the local clouds implies a dark gas mass in the Milky Way comparable to the molecular one.

The census of atomic and molecular gas in the Milky Way mainly comes from the surveys of the 21-cm-HI and 2.6-mm-CO lines. H_2 molecules are not directly observed in the cold molecular clouds, but the velocity-integrated CO intensity, W(CO), empirically scales to the N(H_2) column density by the X = N(H_2)/W(CO) factor. Cold dust, near 16 to 20 K, is mixed in both gas phases, and its thermal emission dominates near 3000 GHz. Colder dust, around 10 K, is seen down to 94 GHz. Dust column densities are traced by optical extinction and reddening measurements. γ rays with energies above 100 MeV are produced by cosmic rays interacting with interstellar gas and radiation, so they can effectively trace the gas mass independent of its chemical or thermodynamic state throughout the Galaxy. These tracers have different limitations and comparing them is essential to map and weigh the main gas reserves of the Milky Way. We have compared them over the whole sky at $5° \leq |b| \leq 80°$, where local clouds dominate and can be mapped in detail.

The HI column-density map, N(HI), combines the 0.5°-resolution Leiden/Dwingeloo survey (*1*) for declinations >–30° with the 1°-resolution data farther south (*2*). The HI lines were assumed to be optically thin. The W(CO) map comes from the Center for Astrophysics compilation at $|b| \leq 32°$ (*3*). The regions outside the survey should be free of bright CO emission (*3*, *4*). The dust intensity map at 3000 GHz, I_{3000}, comes from InfraRed Astronomical Satellite (IRAS) maps calibrated with Diffuse InfraRed Background Experiment (DIRBE) data, with the zodiacal light and point sources removed (*5*). Correcting I_{3000} for color temperature variations yields dust column densities. The reddening [E(B-V)] map (*5*), in magnitudes (mag.), comes from I_{3000} corrected to a temperature of 18.2 K with the use of DIRBE 100- to 240-μm ratios and calibrated to the reddening of elliptical galaxies with a 16% precision. It is consistent with star estimates from the Sloan Digital Sky Survey for E(B-V) < 0.5 (*6*). Only 6% of the region under study exhibits larger reddening. The dust intensity map at 94 GHz, I_{94}, was constructed (*7*) with two modified Planck $\nu^{1.67}$ B_ν (9.4 K) and $\nu^{2.70}$ B_ν (16.2 K) emissivities to match the Cosmic Background Explorer (COBE) Differential Microwave Radiometers (DMR) and Far InfraRed Absolute Spectrophotometer (FIRAS) data. It was successfully compared with the Wilkinson Microwave Anisotropy Probe (WMAP) data at 94 GHz (*8*).

In γ rays, the Energetic Gamma Ray Experiment Telescope (EGRET) archival database provides a 9-year photon count map and an exposure map, ε, for events above 100 MeV and within 30° of the telescope axis. The inverse-Compton (IC) intensity map, I_{IC}, integrated above 100 MeV, comes from the GALPROP 45-600202 model for cosmic-ray propagation in the Galaxy (*9*), and its estimate of the radiation field, which includes the cosmological microwave background (CMB), stellar radiation, and dust radiation with peaks near 100 and 10 μm. Given the EGRET exposure and point-spread function (PSF) above 100 MeV, we produced a map, N_{sou} (SOU), of the photon count contribution from the 138 persistent point sources of the third EGRET catalog (*10*) with a detection significance >5σ at $|b| < 30°$ and >4σ at higher latitudes. We used their 4-year average fluxes. Flaring sources not detected in the 4-year data were not included. The mid-latitude threshold was raised from 4σ to 5σ because the addition of substantial interstellar emission may cast doubts on the importance of the faint sources spatially correlated with gas tracers (*11*). We discarded 24 such sources.

Because energetic cosmic rays can penetrate all gas phases and the γ rays radiate easily away, the γ-ray intensity can be modeled as a linear combination of gas tracers, the IC map, the extragalactic background intensity (I_E), and the point sources. The contribution from the ionized hydrogen is neglected. The modeled photon counts in 0.5° × 0.5° bins, $N_p(l,b) = [q_{HI}\,\mathrm{N(HI)}(l,b) + q_{CO}\,\mathrm{W(CO)}(l,b) + q_{dust}\,I_{dust}(l,b) + q_{IC}\,\mathrm{IIC}(l,b) + I_E]\,\varepsilon(l,b) + q_{SOU}\,N_{sou}(l,b)$, are convolved with the PSF for an input $E^{-2.1}$ spectrum. I_{dust} refers to any of the dust maps. The emissivities, q, were fitted to the γ-ray data for different sets of tracers by means of a maximum-likelihood test with Poisson statistics (*12*) (Table 1). Consistent results were obtained at $|b| \geq 5°$ and 10°, indicating that the derived emissivities are local-medium averages. We checked that they are not biased by the lack of cosmic-ray gradient in the Galactic disk. Different point-source data sets yield <10% variations in q_{dust} and <1% variations in the other parameters. We used complete and residual dust maps; the latter were obtained by removing the part linearly correlated with N(HI) and W(CO) from a χ^2 fit using equal area pixels (*13*). Both give the same maximum-likelihood values and q_{dust}. The residual maps ($I_{3000res}$, $E(B\text{-}V)_{res}$, and I_{94res}) were used to evaluate "dust-free" q_{HI} and q_{CO} γ-ray emissivities.

Compared with earlier studies that used only N(HI) (*5*, *14*), both the I_{94res} and $E(B\text{-}V)_{res}$ maps confirm the existence of extensive coherent regions with apparently large dust-to-gas excesses. Additional gas, seen in γ rays but not in radio, complements the dust. The excesses form large halos systematically surrounding all nearby CO clouds (Fig. 1). By filtering out the large-scale HI contribution from the Galactic disk, we have isolated nearby HI clouds that are closely associated with the excess clouds (Fig. 2). The latter bridge the CO cores to the diffuse HI clouds. They are much more prominent at low frequency than at 3000 GHz, confirming the cold temperatures indicated by the DIRBE, FIRAS, and WMAP data, and they largely contribute to the "anomalous microwave emission" (*5*, *7*, *8*, *14*, *15*). They do not spatially correlate with free-free emission.

Even though dust is mixed in the atomic and molecular phases, the maximum-likelihood tests to the γ-ray data reject the I_{3000} dust map as a single tracer of the whole gas. The N(HI)+W(CO) model yields a much better fit [$2\ln(\lambda) > 13{,}530$]. The maximum-likelihood increase from the N(HI)+W(CO)

[1]Astrophysique Interactions Multi-échelles (CEA/Universite Paris 7/CNRS), Commissanat á l'Energie Atomique, DSM/DAPNIA, Service d'Astrophysique, CEA, Saclay, 91191 Gif sur Yvette, France. [2]Grand Accélérateur National d'Ions Lourds (CEA/CNRS), boulevard Henri Becquerel, BP 55027, 14076 Caen, France. [3]Astroparticules et Cosmologie (CNRS/Université Paris 7/CEA), 11 place Marcellin Berthelot, 75005 Paris, France.

*To whom correspondence should be addressed. E-mail: isabelle.grenier@cea.fr

to the N(HI)+W(CO)+I_{3000} model mostly comes from the Cygnus, Ophiuchus, and Orion A and B clouds. Little γ-ray emission is associated with the I_{3000} map on larger scales. The γ-ray fit largely improves (Fig. 3 and fig. S1) when using the colder dust tracer I_{94} and the dust column densities as traced by the E(B-V) reddening [see the 2ln(λ) values in Table 1].

The q_{HI} emissivity found at $5° \le |b| \le 80°$ is consistent with the solar circle average (±SD) of $(1.60 \pm 0.02) \times 10^{-26}$ s^{-1} sr^{-1} (*16*) and 15% lower than those obtained near major local clouds when neglecting the IC emission (*17*). The extragalactic intensity agrees with that measured with the EGRET interstellar model: $(14.5 \pm 0.5) \times 10^{-6}$ cm^{-2} s^{-1} sr^{-1} (*18*, *19*). It is larger than the $(11.10 \pm 0.12 \pm 2.2) \times 10^{-6}$ cm^{-2} s^{-1} sr^{-1} GALPROP estimate (*20*) because of the 30% lower IC intensity than that in GALPROP (*9*). Provided cosmic rays uniformly pervade the HI and H_2 phases, the N(HI)+W(CO) model yields an average $X_\gamma = q_{CO}/(2q_{HI}) = (1.74 \pm 0.03) \times 10^{20}$ molecules (mol.) cm^{-2} K^{-1} km^{-1} s in the solar neighborhood, fully consistent with the factor $X = (1.8 \pm 0.3) \times 10^{20}$ mol. cm^{-2} K^{-1} km^{-1} s obtained with the temperature-corrected I'_{3000} map and a smoothed I'_{3000}/N(HI) ratio to measure the total gas (*3*). It is close to the Galactic averages of $(1.9 \pm 0.2) \times 10^{20}$ mol. cm^{-2} K^{-1} km^{-1} s (*16*) and $(1.56 \pm 0.05) \times 10^{20}$ mol. cm^{-2} K^{-1} km^{-1} s (*19*) derived from γ rays and different gas models.

The considerable improvement in the γ-ray fits when adding the I_{94} or E(B-V) dust tracers demonstrates that γ rays are produced in the cold dust halos, in excess of those born in the HI and CO gas or in the warmer dust in these directions. Splitting the sky in three longitude intervals did not change the result, so one particular region does not drive the fit. This bright emission, comparable to the entire I_{IC} map, is not due to IC emission from the colder dust in the cloud halos. It contributes only 0.6 and 0.9% of the CMB and warmer dust emissions [for a local electron spectrum $I_e = 708$ (E/1 GeV)$^{-3.3}$ m^{-2} s^{-1} sr^{-1} GeV^{-1} (*21*) and two dust components with $\nu^{1.67}$ B_ν (9.4 K) and $\nu^{2.70}$ B_ν (16.2 K) emissivities scaled to match typical fluxes of 1.5 MJy/sr at 500 GHz (FIRAS) and 15 MJy/sr at 3000 GHz (IRAS)]. The lack of correlation with the 408 MHz synchrotron map shows that GeV cosmic rays are not efficiently trapped in these cloud halos. Their distribution couples to gas density (*19*) and spiral arms (*17*), but their diffusion properties imply coupling lengths much larger than the cloud sizes: 1.76 ± 0.20 kpc for nuclei (*19*) and several hundred parsecs for the highest energy electrons with large radiative losses (*22*). Measurements of q_{HI} indeed yield equivalent cosmic-ray densities within 1 kpc from the Sun (*17*). Because the local dust mass is only 1% of the gas one, hadronic interactions with grains are negligible. The γ rays therefore trace the dark gas forming these cloud halos, a gas invisible in HI, CO, and free-free emission.

Assuming the same cosmic-ray flux in the diffuse dark and HI gas, the γ-ray intensities give dark-gas column densities, NH_{dark} (Fig. 4 and fig. S2). The E(B-V) and I_{94} tracers, total and residual maps, give consistent NH_{dark} column densities within 30% over most regions. Fitting cloud complexes individually may lead

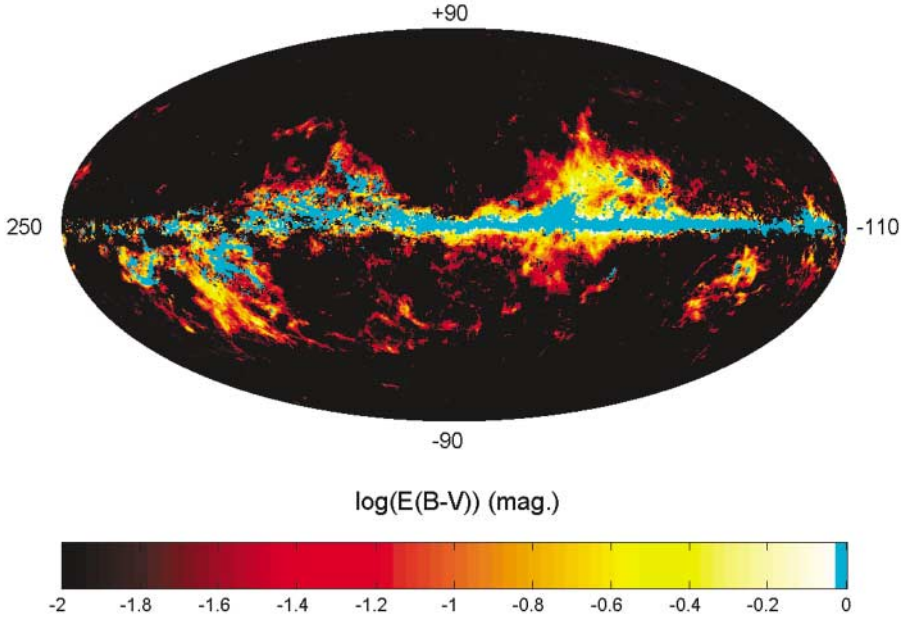

Fig. 1. Map, in Galactic coordinates centered on $l = 70°$, of the excess dust reddening found above that linearly correlated with the integrated HI and CO line intensities. The 94-GHz emission map shows the same excesses. CO intensities above 4 K km s^{-1} are overlaid in cyan. The dust excesses form extended halos around all CO clouds, the bright ones as well as the fainter CO cloudlets that are not overlaid. This dust spreads in a dark gas, not seen in HI and CO but detected in γ rays.

Table 1. Best fits to the γ-ray data at $5° \le |b| \le 80°$ and $10° \le |b| \le 80°$, for the complete and residual (in bold and italics) dust maps. The log-likelihood ratios 2.ln(λ), measuring the fit improvement, are given with respect to the N(HI)+W(CO) gas model and are distributed as a χ^2 with one degree of freedom (*12*). The errors are statistical, not including systematic uncertainties [10% in the EGRET exposure (*10*), 20% in the true N(HI) (*32*) and dust maps (*5*), and 20% in the "dust-free" q_{CO} because of cloud-to-cloud variations in the dust residuals toward the CO clouds].

2.ln(λ)	q_{HI} (10^{-26} s^{-1} sr^{-1})	q_{CO} (10^{-6} cm^{-2} sr^{-1} K^{-1} km^{-1})	q_{EBV} (10^{-6} mag^{-1} cm^{-2} s^{-1} sr^{-1})	q_{I94} (10^{-4} mK^{-1} cm^{-2} s^{-1} sr^{-1})	q_{I3000} (10^{-7} MJy^{-1} cm^{-2} s^{-1})	q_{IC} (10^{-1})	q_{SOU}	I_E (10^{-6} cm^{-2} s^{-1} sr^{-1})
				$5° \le \|b\| \le 80°$				
0	1.62 ± 0.01	5.65 ± 0.10				7.46 ± 0.06	1.01 ± 0.01	13.21 ± 0.09
241.8	***1.63 ± 0.01***	***5.54 ± 0.09***			***2.83 ± 0.20***	***6.54 ± 0.09***	***1.00 ± 0.01***	***13.93 ± 0.10***
1298.0	***1.64 ± 0.01***	***5.82 ± 0.09***		***4.27 ± 0.12***		***6.39 ± 0.07***	***0.96 ± 0.01***	***13.96 ± 0.09***
1556.7	***1.65 ± 0.01***	***5.91 ± 0.09***	***57.5 ± 1.5***			***6.43 ± 0.07***	***0.96 ± 0.01***	***13.91 ± 0.09***
241.8	1.49 ± 0.02	4.84 ± 0.11			2.83 ± 0.21	6.54 ± 0.09	1.00 ± 0.01	13.74 ± 0.10
1298.0	0.77 ± 0.02	1.63 ± 0.15		4.27 ± 0.10		6.39 ± 0.07	0.96 ± 0.01	14.30 ± 0.09
1556.7	0.71 ± 0.04	0.53 ± 0.54	57.5 ± 3.7			6.43 ± 0.07	0.96 ± 0.01	14.45 ± 0.09
				$10° \le \|b\| \le 80°$				
0	1.74 ± 0.02	5.31 ± 0.12				7.90 ± 0.09	0.98 ± 0.01	12.40 ± 0.10
284.4	***1.74 ± 0.02***	***5.28 ± 0.12***			***4.04 ± 0.25***	***7.07 ± 0.10***	***0.97 ± 0.01***	***13.03 ± 0.10***
957.9	***1.75 ± 0.02***	***5.70 ± 0.12***		***4.32 ± 0.14***		***7.25 ± 0.09***	***0.91 ± 0.01***	***12.84 ± 0.10***
1048.6	***1.76 ± 0.02***	***5.60 ± 0.12***	***54.4 ± 1.7***			***7.17 ± 0.09***	***0.91 ± 0.01***	***12.83 ± 0.10***

to 20% variations, but it first requires a careful reanalysis of the point-source fluxes. The gas-to-dust ratio deduced from the amount of dark gas is consistent with the average ratio found in the local CO clouds in (*13*): $[NH/E(B\text{-}V)]_{dark} = (3.5 \pm 0.2) \times 10^{21}$ cm^{-2} mag^{-1} and $[NH/E(B\text{-}V)]_{CO} = (3.72 \pm 0.28) \times 10^{21}$ cm^{-2} mag^{-1}. Both are lower than the average of $(6.17 \pm 0.22) \times 10^{21}$ cm^{-2} mag^{-1} found in the local HI gas, close to the canonical 5.8×10^{21} cm^{-2} mag^{-1} value (*23*), but reflect a metallicity close to normal.

We calculated the masses in the molecular, dark, and atomic phases in seven regions from 140 to 450 pc from the Sun (Table 2), with the use of X_γ, a mean weight per atom of 1.4 times the hydrogen mass, and the CO and HI data in Figs. 1 and 2. We added the masses of CO clouds in the MBM 53-54-55 and Chamaeleon complexes (*24*, *25*) that are not covered by our data (*4*). Because the three phases are spatially connected, their relative masses are independent of distance. The dark-gas mass increases similarly with the independent H_2 and HI mass estimates, approximately as $M^{0.4}$ and $M^{0.5}$, so its relative contribution decreases from small to massive clouds (Table 2 and fig. S3). The sample is small but spans the mass range most typical of Galactic clouds, from translucent 10^3–solar mass ($M_\odot$) clouds to giant complexes $>10^5$ $M_\odot$. In smaller cirrus clouds, there are also comparable masses of HI and dark gas (inferred from dust 3000 GHz emission) without CO detection (*26*). For a uniform X factor, the mass spectrum of Galactic CO clouds follows a power-law $dN/dM_{H2} \propto M_{H2}^{-\alpha}$, where $\alpha = 1.6$ to 1.9 [$\alpha = 1.67 \pm 0.25$ in the first quadrant in the range of $10^{4.5}$ to $10^{6.5}$ $M_\odot$ (*27*) and $\alpha = 1.80 \pm 0.03$ from 600 to 10^6 $M_\odot$ in the outer Galaxy (*28*)]. The best χ^2 power-law fit of M_{dark} with M_{H2} in the local regions, which matches the lowest dark masses and underestimates those in both Aquila regions by a factor of 4, is $M_{dark} = (457 \pm 68) \times (M_{H2}^{0.36 \pm 0.03})$ in solar masses (fig. S3). Together with the CO mass spectrum, it implies a minimum dark-to-molecular mass fraction in the Galaxy of 50 to 100% in the interval of 10^3 to 10^6 $M_\odot$, for $\alpha = 1.6$ to 1.9, respectively. Locally, $M_{dark}/M_{H2} \approx 30\% \approx M_{dark}/M_{HI}$, which should be taken as lower limits because the local sample is strongly biased to high masses with less dark gas (*27*). So the dark-cloud mass in the Galaxy should compare with the molecular one. It strengthens the possibility that cold H_2 substantially contribute to the dark baryonic matter (*29*).

Whether the dark gas is gravitationally bound and dominated by cold HI or H_2 is unclear. H_2 number fractions of 49 to 76% have been found in ultraviolet absorption lines toward three stars in the Chamaeleon clouds, with an H_2 formation time scale of 20 million years less than the photodissociation one (*30*).

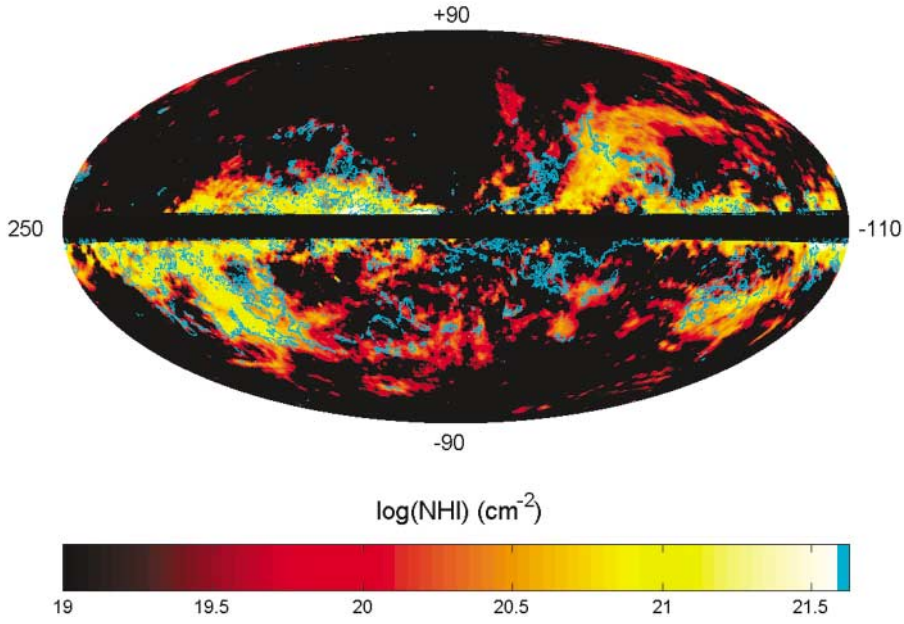

Fig. 2. Map, in Galactic coordinates centered on $l = 70°$, of the HI column densities in nearby atomic clouds isolated by subtracting the Galactic disk emission from the best-fit cosecant law about the warped plane. The outer contour of the dust excesses of Fig. 1 is overlaid in cyan, showing a remarkable association with the atomic clouds.

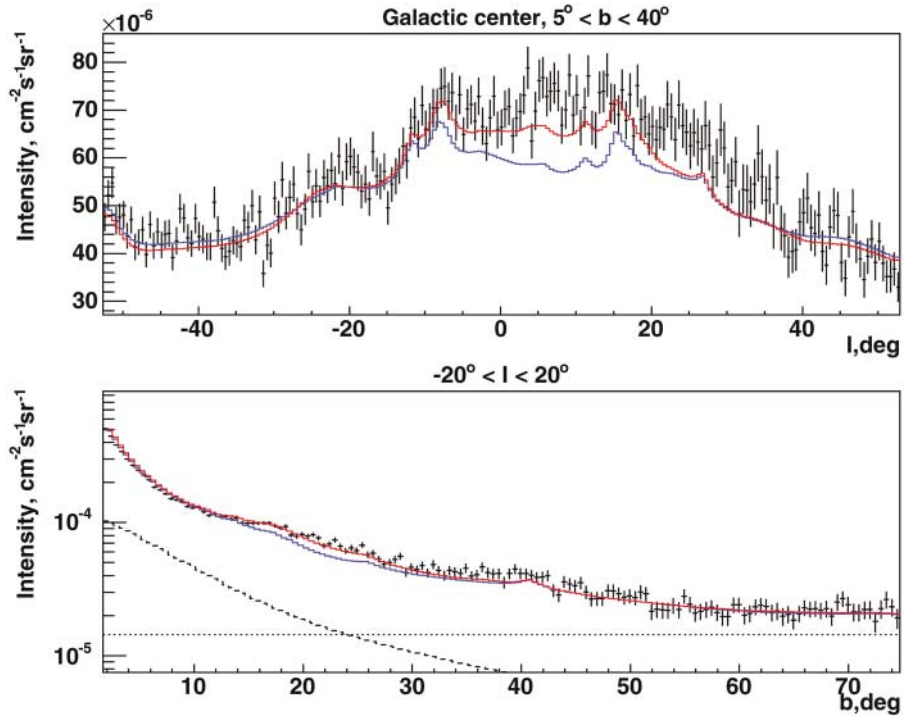

Fig. 3. Longitude (**top**) and latitude (**bottom**) profiles of the observed γ-ray intensity in the Aquila-Ophiuchus-Libra region versus the N(HI)+W(CO) gas model (blue) and the N(HI)+W(CO)+E(B-V) model (red). The dashed and dotted curves (bottom) outline the IC and extragalactic background intensities, respectively. Error bars show mean ± SD.

Larger scales are probed in CO (0.3 pc) and γ rays (1.4 pc). In the direction with no CO detection, the dark gas could contribute half of the H_2 seen in absorption (table S1). The low $[NH/E(B\text{-}V)]_{dark}$ ratio, close to the CO one, also supports a high H_2 abundance. There could be a sharp threshold in extinction ($A_v > 0.25$ mag) before CO is detectable (*31*), but the 0.2- to 1.5-magnitude extinction in the dark clouds provides enough shielding for the molecules. Assuming pure H_2 halos, we find potential CO intensities of 0.5 to 1.5 K km s^{-1}

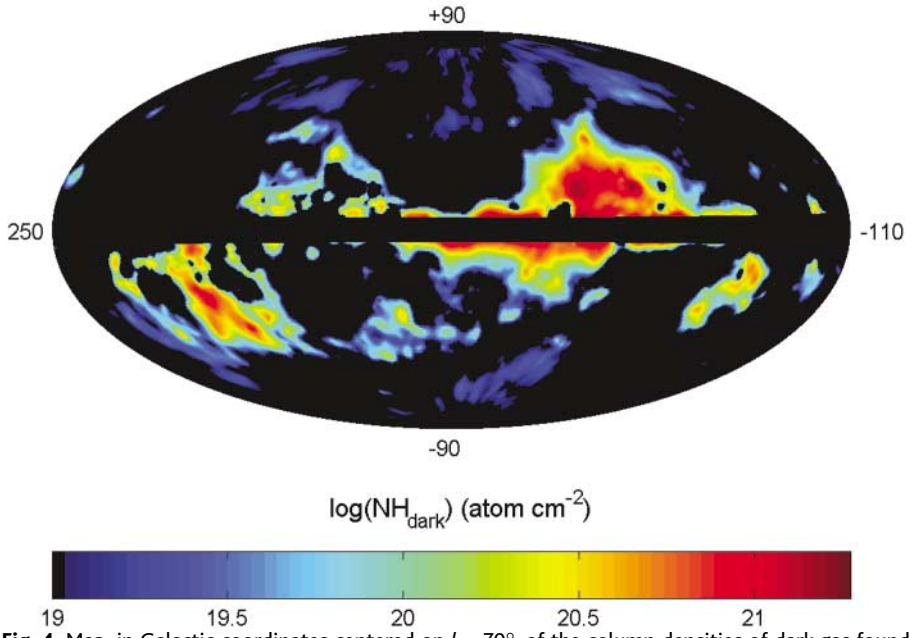

Fig. 4. Map, in Galactic coordinates centered on $l = 70°$, of the column densities of dark gas found in the dust halos, as measured from their γ-ray intensity with the reddening map. This gas complements that visible in HI and CO. The two dust tracers [E(B-V) and 94-GHz emission] yield consistent values within 30% over most regions.

Table 2. Total mass and H_2:dark:HI mass proportions in the CO, dark, and atomic phases in nearby regions.

Region	Longitudes, latitudes	Distance (pc)	Total mass (10^5 $M_\odot$)	H_2:dark:HI
Cepheus-Cassiopeia-Polaris	[80,165] [5, 50]	300	5.4	7.5:1:7.3
Orion	[–163, –134] [–40, –5]	450	4.8	8.6:1:7.3
Aquila-Ophiuchus-Libra	[–70, 50] [5, 60]	140	1.6	0.8:1:1.0
Taurus-Perseus-Triangulum	[140, 197] [–60, –5]	140	1.4	2.3:1:3.1
Aquila-Sagittarius	[–36, 50] [–50, –5]	140	0.43	0.2:1:0.5
Chamaeleon	[–90, –35] [–50, –8]	160	0.40	0.9:1:3.7
Pegasus	[50, 140] [–60, –26]	150	0.16	0.7:1:3.4

in most places, close to the sensitivity of the large-scale surveys for small-size cloudlets, and higher values in the Aquila-Ophiuchus-Libra (2 to 4 K km s^{-1}) and Taurus-Perseus-Triangulum (2 K km s^{-1}) regions where only faint scattered CO cloudlets were detected. On the other hand, the dark clouds may be remnants of the atomic clouds that condensed to form the CO cores or they may be rich in photodissociated gas torn away in the ambient turmoil. Cold HI, not properly accounted for in emission because of its mixing with warm HI lines, has been observed with and without CO. It shows abundant structure in self-absorption, but its extent at medium latitude is unknown. NHI_{warm} and NHI_{cold} column densities have been measured against 65 radio sources (*32*), 22 of which are seen through dark clouds. A weak correlation was found between $NH_{halo}/\sin|b|$ and $NHI_{cold}/\sin|b|$, with a correlation coefficient of 0.67 ± 0.09. None was found with NHI_{warm}. So, whereas the dark gas provides a key link in the evolution between the atomic and molecular clouds, the nature of its major constituent is unknown.

The addition of substantial mass to the interstellar γ-ray emission implies that the cosmic-ray densities estimates are currently overestimated in regions rich in dark gas, away from the giant molecular complexes. This should steepen the cosmic-ray gradient with Galactocentric radius and enhance the arm-interarm contrast in cosmic rays. Yet, resolving the dark clouds in the Galactic disk, with dust temperature gradients near bright OB associations along crowded lines of sight and poor angular resolution in γ rays, is a difficult but important challenge. The presence of dark clouds to high latitudes also implies significant revisions of the EGRET catalog of γ-ray sources.

References and Notes

1. D. Hartmann, W. B. Burton, *Atlas of Galactic Neutral Hydrogen* (Cambridge Univ. Press, Cambridge, 1997).
2. J. M. Dickey, F. J. Lockman, *Annu. Rev. Astron. Astrophys.* **28**, 215 (1990).
3. T. M. Dame, D. Hartmann, P. Thaddeus, *Astrophys. J.* **547**, 792 (2001).
4. T. M. Dame, P. Thaddeus, in *Milky Way Surveys: The Structure and Evolution of Our Galaxy*, D. Clemens, T. Brainerd, Eds. (ASP Conference Series, Astronomical Society of the Pacific, San Francisco, CA, 2004), pp. 66–72.
5. D. J. Schlegel, D. P. Finkbeiner, M. Davis, *Astrophys. J.* **500**, 525 (1998).
6. D. P. Finkbeiner *et al.*, *Bull. Am. Astron. Soc.* **36**, 2 (2004).
7. D. P. Finkbeiner, M. Davis, D. J. Schlegel, *Astrophys. J.* **524**, 867 (1999).
8. D. P. Finkbeiner, *Astrophys. J.* **614**, 186 (2004).
9. A. W. Strong, I. V. Moskalenko, O. Reimer, *Astrophys. J.* **613**, 962 (2004).
10. R. C. Hartman *et al.*, *Astrophys. J. Suppl. Ser.* **123**, 79 (1999).
11. I. Grenier, *Astron. Astrophys.* **364**, L93 (2000).
12. W. T. Eadie, D. Drijard, F. James, M. Roos, B. Sadoulet, *Statistical Methods in Experimental Physics* (North-Holland, Amsterdam, 1971).
13. The best linear fits to the dust data at $5° \leq |b| \leq 80°$, in equal area pixels of 1.6×10^{-5} sr, follow. We used $\sigma_{HI} = 3 \times 10^{18}$ cm^{-2}, $\sigma_{CO} = 0.6$ K km s^{-1}, and $\sigma_{dust}/I_{dust} = 0.2$. N(HI) is in units of centimeters^{-2}, W(CO) is in kelvin kilometer seconds, E(B-V) is in magnitude, I_{94} is in millikelvins, and I_{3000} in megajansky per steradian. The following equations show the best linear fits:

$$E(B\text{-}V) = (1.62 \pm 0.06) \times 10^{-22}\ N(HI) + (9.4 \pm 0.7) \times 10^{-2}\ W(CO) - (9.4 \pm 0.3) \times 10^{-3}$$

$$I_{94} = (2.04 \pm 0.04) \times 10^{-23}\ N(HI) + (9.8 \pm 0.7) \times 10^{-3}\ W(CO) - (8.0 \pm 1.5) \times 10^{-4}$$

$$I_{3000} = (4.9 \pm 0.1) \times 10^{-21}\ N(HI) + (2.5 \pm 0.5) \times W(CO) + (0.7 \pm 0.4)$$

14. G. Lagache, A. Abergel, F. Boulanger, J.-L. Puget, *Astron. Astrophys.* **333**, 709 (1998).
15. G. Lagache, *Astron. Astrophys.* **405**, 813 (2003).
16. A. W. Strong, J. R. Mattox, *Astron. Astrophys.* **308**, L21 (1996).
17. S. Digel, I. A. Grenier, S. D. Hunter, T. M. Dame, P. Thaddeus, *Astrophys. J.* **555**, 12 (2001).
18. P. Sreekumar *et al.*, *Astrophys. J.* **494**, 523 (1998).
19. S. D. Hunter *et al.*, *Astrophys. J.* **481**, 205 (1997).
20. A. W. Strong, I. V. Moskalenko, O. Reimer, *Astrophys. J.* **613**, 956 (2004).
21. C. Fichtel, R. G. Stone, M. E. Ozel, P. Sreekumar, *Astrophys. J.* **374**, 134 (1991).
22. M. Pohl, C. Perrot, I. Grenier, S. Digel, *Astron. Astrophys.* **409**, 581 (2003).
23. R. C. Bohlin, B. D. Savage, J. F. Drake, *Astrophys. J.* **224**, 132 (1978).
24. H. Yamamoto, T. Onishi, A. Mizuno, Y. Fukui, *Astrophys. J.* **592**, 217 (2003).
25. A. Mizuno *et al.*, *Publ. Astron. Soc. Jpn.* **53**, 971 (2001).
26. W. T. Reach, B.-C. Koo, C. Heiles, *Astrophys. J.* **429**, 672 (1994).
27. J. P. Williams, C. F. McKee, *Astrophys. J.* **476**, 166 (1997).
28. M. H. Heyer, J. M. Carpenter, R. L. Snell, *Astrophys. J.* **551**, 852 (2001).
29. F. Combes, *New Astron. Rev.* **46**, 755 (2002).
30. C. Gry *et al.*, *Astron. Astrophys.* **391**, 675 (2002).
31. L. Blitz, D. Bazel, F. X. Désert, *Astrophys. J.* **352**, L13 (1990).
32. C. Heiles, T. H. Troland, *Astrophys. J.* **586**, 1067 (2003).

33. We thank A. Strong, I. Moskalenko, and O. Reimer for providing their IC emission maps and the referees for their insightful remarks. Discussions with F. Boulanger, C. Heiles, J. L. Puget, M. Sauvage, and H. Aussel were extremely helpful. This research made use of the Legacy Archive for Microwave Background Data Analysis (LAMBDA) and High-Energy Astrophysics Science Archive Research Center (HEASARC) archives from NASA.

Supporting Online Material

www.sciencemag.org/cgi/content/full/307/5713/1292/DC1
Figs. S1 to S3
Table S1

29 October 2004; accepted 3 January 2005
10.1126/science.1106924